Maniatis, T., Fritsch, E. F., & Sambrook, J. (1982) in *Molecular Cloning: a Laboratory Manual*, Cold Spring Harbor Laboratory, Cold Spring Harbor, NY.
Matsuzawa, H., Asoh, S., Kunai, K., Muraiso, K., Takasuga, A., & Ohta, T. (1989) *J. Bacteriol. 171*, 558-560.
Messing, J. (1983) *Methods Enzymol. 101*, 20-78.
Moews, P. C., Knox, J. R., Dideberg, O., Charlier, P., & Frère, J.-M. (1990) *Proteins 7*, 156-171.
Murphy, B. P., & Pratt, R. F. (1988) *Biochem. J. 256*, 667-672.
Nakagawa, J., Tamaki, S., Tomioka, S., & Matsuhashi, M. (1984) *J. Biol. Chem. 259*, 13937-13946.
Nakamura, K., & Inouye, M. (1982) *EMBO J. 1*, 771-775.
Nakamura, M., Maruyama, I. N., Soma, M., Kato, J., Suzuki, H., & Hirota, Y. (1983) *Mol. Gen. Genet. 191*, 1-9.
Nicholas, R. A., Ishino, F., Park, W., Matsuhashi, M., & Strominger, J. L. (1985a) *J. Biol. Chem. 260*, 6394-6397.
Nicholas, R. A., Suzuki, H., Hirota, Y., & Strominger, J. L. (1985b) *Biochemistry 24*, 3448-3453.
Nicholas, R. A., Strominger, J. L., Suzuki, H., & Hirota, Y. (1985c) *J. Bacteriol.*, 456-460.
Oefner, C., D'Arcy, A., Daly, J. J., Gubernator, K., Charnas, R. L., Heinze, I., Hubschwerlen, C., & Winkler, F. K. (1990) *Nature 343*, 284-288.
Ogura, T., Bouloc, P., Niki, H., D'Ari, R., Hiraga, S. & Jaffé, A. (1989) *J. Bacteriol. 171*, 3025-3030.
Samraoui, B., Sutton, B. J., Todd, R. J., Artymiuk, P. J., Waley, S. G., & Phillips, D. C. (1986) *Nature 320*, 378-380.
Schiffer, M., & Edmundson, A. B. (1967) *Biophys. J. 7*, 121-135.
Spratt, B. G. (1975) *Proc. Natl. Acad. Sci. U.S.A. 72*, 2999-3003.
Spratt, B. G. (1977) *Eur. J. Biochem. 72*, 341-352.
Sutcliffe, J. G. (1978) *Proc. Natl. Acad. Sci. U.S.A. 75*, 3737-3741.
Takasuga, A., Adachi, H., Ishino, F., Matsuhashi, M., Ohta, T., & Matsuzawa, H. (1988) *J. Biochem. 104*, 822-826.
Tamaki, S., Matsuzawa, H., & Matsuhashi, M. (1980) *J. Bacteriol. 141*, 52-57.
Taylor, J. W., Ott, J., & Eckstein, F. (1985) *Nucleic Acids Res. 13*, 8765-8785.
Tipper, D. J., & Strominger, J. L. (1965) *Proc. Natl. Acad. Sci. U.S.A. 54*, 1133-1141.
Tsukamoto, K., Tachibana, K., Yamazaki, N., Ishii, Y., Ujiie, K., Nishida, N., & Sawai, T. (1990) *Eur. J. Biochem. 188*, 15-22.
Varetto, L., Frère, J.-M., Nguyen-Distèche, M., Ghuysen, J.-M., & Houssier, C. (1987) *Eur. J. Biochem. 162*, 525-531.
Vieira, J., & Messing, J. (1987) *Methods Enzymol. 153*, 3-11.
Waxman, D. J., & Strominger, J. L. (1983) *Annu. Rev. Biochem. 52*, 825-869.
Yanisch-Perron, C., Vieira, J., & Messing, J. (1985) *Gene 33*, 103-119.
Yocum, R. R., Waxman, D. J., Rasmussen, J. R., & Strominger, J. L. (1979) *Proc. Natl. Acad. Sci. U.S.A. 76*, 2730-2734.

Solution Structure of Phosphorylase Kinase Studied Using Small-Angle X-ray and Neutron Scattering†

S. J. Henderson,‡ P. Newsholme,§ D. B. Heidorn,‡,∥ R. Mitchell,§ P. A. Seeger,‡ D. A. Walsh,§ and J. Trewhella*,‡
Life Sciences Division and LANSCE, Los Alamos National Laboratory, Los Alamos, New Mexico 87545, and Department of Biological Chemistry, University of California, Davis, California 95616
Received July 24, 1991; Revised Manuscript Received September 26, 1991

ABSTRACT: Small-angle X-ray and neutron scattering have been used to characterize the solution structure of rabbit skeletal phosphorylase kinase. The radius of gyration of the unactivated holoenzyme determined from neutron scattering is 94 Å, and its maximum dimension is approximately 275-295 Å. A planar model has been constructed that is in general agreement with the dimensions of the transmission electron microscope images of negatively stained phosphorylase kinase and that gives values for the radius of gyration, maximum linear dimension, and a pair distribution function for the structure that are consistent with the scattering data.

Phosphorylase kinase (PhK)[1] is a large complex molecule (approximately 1.3×10^6 Da) that consists of 16 subunits, made up of four identical copies of four different polypeptides denoted α, β, γ, and δ, with molecular weights 138 422, 125 294, 44 637, and 16 680, respectively [for a review, see Pickett-Gies and Walsh (1986)]. The γ-subunit contains the catalytic site. The δ-subunit is identical to calmodulin, confers Ca^{2+} sensitivity to the enzyme, and is the primary mode whereby the enzyme is regulated by Ca^{2+} in response to neural and hormonal signals. Both the α- and β-subunits are regulatory and are phosphorylated by either the cAMP-dependent

† This work was performed under the auspices of the DOE (Contract W-7405-ENG-36) and is supported by NIH Grants GM40528 (J.T.) and DK13613 (D.A.W.) and by DOE/Office of Health and Environmental Research project KP-04-01-00-0 (J.T.). This work has benefited from the use of facilities at the Manuel Lujan Jr. Neutron Scattering Center, a national user facility funded as such by DOE/Office of Basic Energy Sciences.
* Author to whom correspondence should be addressed.
‡ Los Alamos National Laboratory.
§ University of California, Davis.
∥ Present address: St. Joseph's Regional Medical Center, Lewiston, ID 83501.

[1] Abbreviations: AFM, atomic force microscopy; c, protein concentration; d_{max}, maximum linear dimension; EDTA, ethylenediaminetetraacetic acid; EGTA, ethylene glycol bis(β-aminoethyl ether)-*N,N,N',N'*-tetraacetic acid; I_0, forward scatter or scattered intensity at zero scattering angle; LQD, low-Q diffractometer; PhK, phosphorylase kinase; R_g, radius of gyration; STEM, scanning transmission electron microscopy; STM, scanning tunneling microscopy; TEM, transmission electron microscopy.

0006-2960/92/0431-437$03.00/0

protein kinase or by autophosphorylation. This phosphorylation is the second major mechanism for regulating PhK in response to hormonal stimulation. The enzyme catalyzes the phosphorylation of phosphorylase, leading to its activation and the consequential degradation of glycogen for metabolic energy. Still only very little is known about the structure of the holoenzyme. Images of PhK suggest that the subunits are arranged as a dimer of octamers $(\alpha_2\beta_2\gamma_2\delta_2)_2$ (Trempe et al., 1986). In electron micrographs (Trempe et al., 1986; Cohen, 1978) the protein appears as a bilobal "butterfly" structure, each half of which might be one of the octamers, with the bridge between the two octamers possibly being comprised of the β-subunits. Atomic force microscopy (AFM) and scanning tunneling microscopy (STM) also indicate a bilobal structure (Edstrom et al., 1989, 1990). A more definitive knowledge of PhK structure is important to understanding its function.

Small-angle scattering from macromolecules can give information about their overall shapes in solution (Heidorn & Trewhella, 1990). We have previously used small-angle scattering to study the interactions of the subunits of PhK. In particular, we characterized large conformational changes in the δ-subunit (calmodulin) of PhK when complexed with the two calmodulin-binding domains in the γ-subunit of PhK (Trewhella et al., 1990). The experiments reported here were aimed at characterizing the holoenzyme, with particular interest in determining whether the bilobal "butterfly" shape seen in the various images of PhK is consistent with solution scattering data. We also measured scattering data for different activation states of PhK in order to determine if there were global structural rearrangements upon activation.

Materials and Methods

Sample Preparation. Phosphorylase kinase was purified from rabbit skeletal muscle by the procedures we have detailed previously (Pickett-Gies & Walsh, 1985). The last step of this purification is zonal sucrose gradient ultracentrifugation. The pure protein produced by this method was monodisperse, as evaluated by a second sucrose gradient ultracentrifugation. When examined by SDS–gel electrophoresis using high amounts of protein (25–50 μg, staining by Coomassie), the preparation contained no quantifiable contaminants (<1%). Further characteristics of the preparation are given in Pickett-Gies and Walsh (1985). Samples were concentrated by vacuum dialysis. For neutron scattering the preparation was dialyzed against D_2O solutions containing 10 mM sodium phosphate buffer, pH 7.0, with 5% sucrose. The final concentration of unactivated PhK was 2.3 mg/mL. D_2O was used to minimize the large incoherent neutron scattering contribution from hydrogen. Samples for X-ray scattering were in H_2O with 10 mM phosphate buffer, pH 7.0, and 4% sucrose. The final concentration of the PhK was 4.4 mg/mL. Protein concentrations were determined by Lowry standardized to absorption at 280 nm (Pickett-Gies & Walsh, 1985). Activated forms of PhK were prepared either by the addition of 16 mol equiv of Ca^{2+} or 4 mol equiv of $4Ca^{2+}$·calmodulin or by cAMP-dependent phosphorylation. The phosphorylation was performed by the incubation of 2.62 mg/mL PhK with 2 μg/mL bovine heart cAMP-dependent protein kinase catalytic subunit, 1 mM EGTA, 3 mM $MgCl_2$, 1 mM ATP for 30 min at 30 °C to achieve fully phosphorylated protein (Ramachandran et al., 1987). The reaction was terminated by addition of EDTA to 20 mM final concentration.

Neutron-Scattering Data Acquisition. The neutron-scattering data were collected at room temperature using the low-Q diffractometer (LQD) at the Manuel Lujan Jr. Scattering Center (LANSCE). The LQD is described in detail in Seeger et al. (1990). The neutron source at LANSCE is a pulsed source and neutron time-of-flight is used to determine the wavelength of each neutron detected in the small-angle scattering experiment. At the time of the experiments reported here, the neutron pulses were delivered at 12 Hz, rather than the 20 Hz currently used, and hence there was less pulse overlap and more usable long wavelength neutrons. As a result, it was possible to measure data at very small values of the scattering vector Q (see below), which greatly facilitated the accurate determination of the relatively large structural parameters for PhK. At the time of the measurements reported here, the LQD did not have an MgO filter to remove very high energy (short wavelength) neutrons from the beam. This resulted in high backgrounds at early times (short wavelengths) in the neutron pulse, and so these data were excluded in the data reduction. The neutron wavelength range used in the data reduction was from 2.75 to 15.4 Å.

X-ray Data Acquisition. X-ray data were collected at room temperature using the small-angle X-ray scattering station at Los Alamos, which is described in detail in Heidorn and Trewhella (1988). The sample-to-detector distance was 63.5 cm.

Small-Angle Scattering Data Analysis. Neutron and X-ray scattering data were reduced to $I(Q)$ vs Q for analysis. $I(Q)$ is the scattered neutron or X-ray intensity per unit solid angle, and Q is the scattering vector, or momentum transfer of the scattering event, and is equal to $4\pi(\sin\theta)/\lambda$, where 2θ is the scattering angle and λ is the neutron or X-ray wavelength. The neutron data were reduced as described in Heidorn et al. (1989) except the spectra were normalized to counts measured by a ^{6}LiF monitor mounted in the beam stop directly in front of the detector. The treatment of the X-ray scattering data is described in Heidorn and Trewhella (1988). Guinier (1939) and indirect Fourier transform [or $P(r)$] (Moore, 1980) analyses were used to calculate radius of gyration, R_g, forward scatter, I_0, and vector distribution functions, $P(r)$, for PhK as described in Heidorn et al. (1989), except in this case high Q data were assumed to extrapolate as Q^{-4} in order to reduce truncation errors in the $P(r)$ transformation (Trewhella et al., 1990).

The radius of gyration for a homogeneous scattering particle is the root-mean-square of the distances of all elemental scattering volumes from the center of mass of the particle and is analogous to the radius of inertia for a rigid body. Guinier (1939) showed that the intensity of the innermost portion of the scattering profile can be approximated well by a Gaussian curve:

$$I(Q) = I_0 \exp(-R_g^2Q^2/3) \quad (1)$$

For globular objects this approximation is typically valid for $QR_g < 1.3$. From eq 1 it can be seen that a plot of ln $I(Q)$ vs Q^2 gives a straight line with slope $-R_g^2/3$ and an extrapolated intercept ln I_0. The vector, or pair, distribution function for a homogeneous scattering particle is the frequency distribution of distances between finite volume elements within the particle and is calculated as the inverse Fourier transform of the scattering profile:

$$P(r) = r^2/2\pi^2 \int I(Q)Q^2 (\sin Qr)/Qr \, dQ \quad (2)$$

The vector distribution function goes to zero at a value corresponding to the maximum dimension of the particle, d_{max}. R_g and I_0 can also be calculated from the second and zeroth moments, respectively, of $P(r)$ [reviewed in Heidorn and Trewhella (1990)].

For flat particles with in-plane dimensions much larger than their thickness, a one-dimensional radius of gyration of

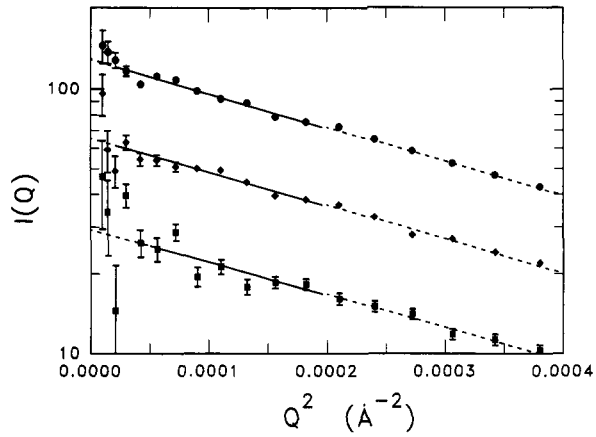

FIGURE 1: Guinier plots of neutron-scattering data from 2.3 (●), 1.2 (◆), and 0.6 (■) mg/mL PhK with 5% sucrose in D_2O.

thickness, R_t, can be determined from the slope of the straight line fit of a semilog plot of scattering data $Q^2I(Q)$ vs Q^2 (Glatter, 1982). As the ratio of the planar dimensions to the mean thickness of the particle becomes smaller, then the lowest Q data will be affected more by the overall radius of gyration of the particle and the linearity is expected to break down at low Q values.

Modeling. The program BIOMOD was written in Turbo-Pascal for an IBM compatible personal computer to generate models of phosphorylase kinase. The program calculates vector distribution functions using methods similar to that described in Heidorn and Trewhella (1988). The program uses a Monte Carlo integration method to calculate the vector distribution functions for models constructed from different types of geometrical building blocks. The block types available include ellipsoids, semiellipsoids, elliptical cylinders, helices, rectangular cubes, and triangular prisms. The program generates random points within the model envelope and calculates the distribution of pairwise distances between these points. Each building block is assigned a uniform scattering density. The program thus calculates vector distribution functions for complicated shaped objects, allowing classes of models to be screened very rapidly. Analytical approaches to these types of calculations would be too slow to be practical.

Results and Discussion

Scattering Data. X-ray scattering data were collected for unactivated PhK and for PhK in various states of activation. The first X-ray data were collected using samples that containd no sucrose. For unactivated PhK in the absence of sucrose, there was clear evidence for protein aggregation in the form of upward curvature of the Guinier plot (see eq 1) at low Q for PhK concentrations greater than 1.85 mg/mL. At 1.85 mg/mL the upward curvature was not evident, but the R_g values were about 8% larger than was generally observed in the presence of sucrose in later X-ray scattering experiments. Addition of Ca^{2+} to the 1.85 mg/mL sample resulted in aggregation even at this concentration of PhK as evidenced by upward curvature of the data in the Guinier plots. The presence of sucrose stabilizes the unactivated PhK monomers and inhibits aggregation, though if samples are left for long periods (more than a week) in 4–5% sucrose, they do begin to show signs of aggregation. All subsequent X-ray and neutron-scattering experiments on PhK were performed on PhK samples freshly prepared in the presence of 4–5% final sucrose concentration.

Neutron-scattering data were collected for unactivated PhK in 5% sucrose at three different protein concentrations. The

Table I: Structural Parameters Determined from Scattering Data for Unactivated PhK

PhK concentration (mg/mL)	d_{max} (Å)	R_g (Å)	I_0/c^a (arb. units)	Q range[b] ($Å^{-1}$)	χ^{2b}
Neutron-Scattering Results					
Guinier analysis					
2.3		94 ± 2.6	56 ± 2.4	0.005–0.014	1.8
1.2		94 ± 3.9	54 ± 4.0	0.005–0.014	1.2
0.6		92 ● 9.5	48 ± 8.0	0.007–0.014	2.7
$P(r)$ analysis					
2.3	275	94 ± 0.8	56 ± 1.7	0.005–0.1	1.29
1.2	295	97 ± 1.3	57 ± 3.4	0.005–0.08	0.94
0.6	280	98 ● 2.4	52 ± 6.0	0.005–0.08	0.93
X-ray Scattering Results					
Guinier analysis					
4.4		101 ± 1.0		0.005–0.014	
$P(r)$ analysis					
4.4	305	102 ± 1.1		0.0085–0.12	1.59

[a] The errors are calculated from the counting statistics and the uncertainty in the PhK concentration (approximately ±0.05 mg/mL). [b] The Q range is that used in the analysis of each data set, and the χ^2 value is the reduced χ^2 for each fit.

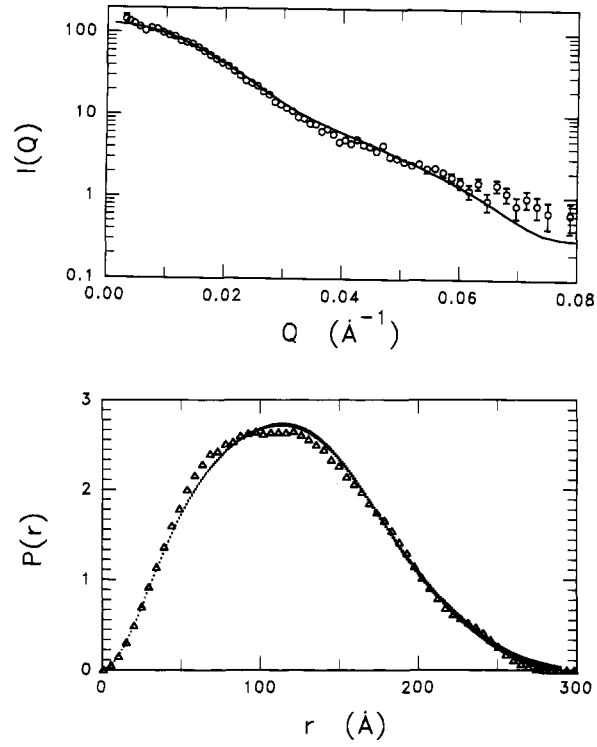

FIGURE 2: Comparison of (a, top) the neutron-scattering data from 2.3 mg/mL PhK with 5% sucrose in D_2O (○) with that calculated for the model depicted in Figure 4 (solid line); (b, bottom) the $P(r)$ function calculated to best fit the scattering data (vertical bars) shown in Figure 2 with that derived from the model (△) depicted in Figure 4. The Q range for the $P(r)$ fit to the scattering data was 0.0046–0.0809 $Å^{-1}$, d_{max} for the $P(r)$ shown was 290 Å, and seven coefficients were determined. The χ^2 for the fit was 1.3 (for 58 degrees of freedom), and the propagated statistical errors are indicated by the height of the vertical bars.

structural parameters derived from Guinier and $P(r)$ analyses of the neutron data, given in Table I, are in good agreement with each other. The uncertainties quoted are based on counting statistics only. Figure 1 shows a Guinier plot of the neutron-scattering data for each PhK sample. Figure 2 shows the neutron-scattered intensity data for unactivated PhK at 2.3 mg/mL over the entire measured Q range and the vector

distribution function, $P(r)$, calculated to best fit those data. The Guinier plots are linear for each sample and show no evidence for upward curvature at low angle. In addition, the linearity extends to higher Q values, well beyond the valid Guinier region, though the parameters given in Table I were determined using only data in the valid Guinier region (i.e., for $QR_g < 1.3$ indicated by the solid lines in the figure). The R_g values show no significant concentration dependence over the range of concentrations measured (0.6–2.3 mg/mL). In addition, I_0/c where c is PhK concentration is constant within experimental uncertainty over the concentration range measured as expected for scattering from particles with the same molecular weight (Kringbaum & Kugler, 1970). These results are consistent with the ultracentrifugation data that indicate the samples were monodisperse.

The uncertainty in d_{max} is difficult to estimate for the neutron data. The parameter d_{max} is determined from the $P(r)$ fitting procedure [see Materials and Methods in Heidorn et al. (1989)]. The spread of values between 275 and 290 Å quoted for the different concentrations of PhK is not considered significant. The statistical quality of the scattering data, particularly at higher Q values (beyond the Guinier region), obtained for the samples with the two lower PhK concentrations is sufficiently worse than the 2.3 mg/mL data that preference should be given to the $P(r)$ parameters determined for the highest PhK concentration.

Table I also gives the results of the Guinier and $P(r)$ analyses for X-ray scattering data from unactivated PhK in 4% sucrose. The R_g and d_{max} values obtained are approximately 8.5% larger than those obtained from the neutron data. Differences are expected between the values determined for R_g using X-ray and neutron scattering. The contrast between the protein and solvent is greater for neutrons compared with X-rays. As a result, contributions to the scattering due to hydration layer effects can be significantly greater in the case of X-ray scattering compared with neutron scattering. Hydration layer effects arise from the fact that macromolecules in solution perturb the solvent at their surfaces, giving rise to differences between the surface solvent and the bulk solvent. These differences can give rise to contrast between the bulk solvent and the layer of solvent perturbed by the protein surface (Zaccai et al., 1986), causing the particle to appear larger than it is. R_g values derived from neutron and X-ray scattering are also affected differently by the distribution of chemical groups within a scattering particle which can give rise to internal density fluctuations. In particular, the hydrophobic core of a protein complex can have a significantly different neutron-scattering density than a surface layer that contains more hydrophilic groups. In the case of X-rays, there is generally less variation in the electron density and hence the X-ray scattering density between these two regions. Another source for the discrepancy between the neutron and X-ray R_g values could be in the different beam geometries used for the experiments. The neutron experiment was done using a point source, while the X-ray experiment used a slit source. In order to derive the structural parameters for the scattering particle from the X-ray data, a correction has to be applied to account for the shape of the beam profile (Moore, 1980). This correction is quite large for particles with large R_g values like PhK and is a potential source of systematic error. Finally, the neutron data extend to significantly lower Q values than do the X-ray data, and hence the large R_g and d_{max} values for PhK would be better determined by the neutron data. The $P(r)$ function derived from the X-ray data for unactivated PhK (not shown) is, however, as expected, very similar to that obtained from the neutron data.

A number of attempts were made to characterize the structure of activated PhK using X-ray scattering. Activation was achieved by either phosphorylation, addition of Ca^{2+}, or addition of $4Ca^{2+}$·calmodulin. In each case, an increase in R_g was observed upon activation, but this increase was always accompanied by an increase in I_0/c. For example, a PhK preparation identical to that used to obtain the X-ray data given in Table I was used to prepare activated PhK by phosphorylation. Analysis of the X-ray scattering data from the phosphorylated PhK indicated that the R_g had increased by 24%, but this was accompanied by an increase in I_0/c of 45%. I_0/c is directly proportional to the molecular weight of the scattering particle, for particles with similar mean scattering densities (Kringbaum & Kugler, 1970); hence, the increase in R_g appears to be due to association of PhK molecules. This conclusion was supported by the fact that when the X-ray scattering curves for the unactivated and activated PhK samples were compared, they differed significantly only in the very low Q regime, where aggregation effects would predominate. This aggregation of PhK might be facilitated by the exposure of hydrophobic sites in the holoenzyme due to conformational changes that may be important in the regulation of PhK activity. Hydrophobic interactions can provide forces strong enough to cause protein association. This type of interaction has been proposed to be important in other calcium-regulated systems. For example, the binding of calmodulin to its various target enzymes is associated with the exposure of hydrophobic sites upon Ca^{2+}-binding to calmodulin (LaPorte et al., 1980; Tanaka & Hidaka, 1980; Babu et al., 1988).

Modeling. The R_g, d_{max} values, and $P(r)$ function for unactivated PhK provide constraints on the structure that can be used to construct models to test against the scattering data. The neutron scattering data from the 2.3 mg/mL sample are the best quality, as well as being the least affected by hydration layer effects, and so these were used for comparison to the model calculations. The simplest model to construct, and the one most readily eliminated, is that of a simple spherical model with a volume appropriate for the molecular weight of PhK. Such a model would give an R_g value of 56 Å and a d_{max} of approximately 143 Å. Both of these values are significantly smaller than is measured for the particle, indicating the molecule must be more extended. Since PhK is made up of a tetramer of tetramers or possibly a dimer of octamers, a number of models were constructed with either tetrahedral or square planar symmetry. For each of these symmetries, when the four tetrameric subunits were modeled as spheres, the R_g and d_{max} values were again too small. In order to obtain larger R_g values, the subunit had to be more elongated and so prolate ellipsoids were considered. While it was possible to model correctly the R_g and d_{max} values with this type of model, it was not possible to model the experimentally derived $P(r)$ function. In particular, the model $P(r)$ functions consistently showed a strong peak near the value of the cross-sectional radius for the ellipsoids which is not evident in the experimental $P(r)$ functions.

In addition to the parameters determined by solution scattering, there are a number of published images obtained using a variety of techniques (Cohen, 1978; Jennissen & Schramm, 1981; Schramm & Jennissen, 1985; Trempe et al., 1986, Edstrom et al., 1989, 1990) that can provide input for the modeling. All of the published images of PhK show a bilobal structure, referred to first by Cohen as a "butterfly" shape. In each case the dimensions of the planar images are

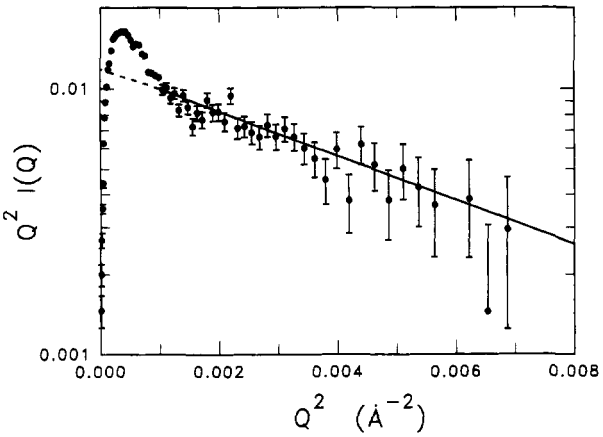

FIGURE 3: Guinier plot for sheet-like forms for the neutron-scattering data from 2.3 mg/mL PhK with 5% sucrose in D_2O. The linear fit over the Q range 0.032–0.097 Å^{-1} gives a radius of gyration of thickness of 13.75 ± 0.59 Å. The χ^2 for the fit is 1.15 (for 35 degrees of freedom).

sufficiently large that the molecules would have to be relatively thin in the third dimension in order to have a reasonable molecular volume. Figure 3 shows the unactivated PhK scattering data plotted for a lamellar form (see Materials and Methods). In the region Q = 0.032–0.097 Å^{-1}, the data are linear as expected for a planar object, and the value obtained for R_t is 13.75 ± 0.59 Å. Below Q = 0.03 Å^{-1}, the linearity breaks down as expected for a planar object having a relatively small ratio between its planar dimensions and mean thickness. Planar models were therefore next constructed on the basis of the various published images of PhK.

The STM and AFM images have maximum dimensions in the plane of the images [≈400 Å from STM image and ≈350 Å from AFM image (Edstrom et al., 1990)] that are significantly larger than the d_{max} values determined from the $P(r)$ functions calculated using either X-ray or neutron-scattering data (275–305 Å). The R_g values calculated for any models with these planar dimensions are correspondingly larger than the values determined from the small-angle scattering data. Emphasis was therefore placed on models that were based on the dimensions of the smaller transmission electron microscope (TEM) images of negatively stained PhK or the scanning transmission electron microscope (STEM) images of unstained PhK.

Trempe et al. (1986) describe their electron microscope images as "resembling two bridged opposing parentheses". Each lobe of this structure is, on average, 200 × 100 Å when negatively stained samples are viewed by conventional transmission electron microscopy. When unstained samples are viewed by scanning transmission electron microscopy, the lobes appear to be 160 × 70 Å. Models were therefore constructed from two opposing parentheses with planar dimensions taken from either of these electron microscope images. The cross-section of each parenthesis was that of a prolate ellipsoid with the length of the semiaxis perpendicular to the plane of the images chosen to give a reasonable value for the molecular volume. Similar to the case for the tetrahedral models, it was possible to model the experimental R_g and d_{max} with this class of model, but there was again a strong peak in the $P(r)$ function at distances near the mean cross-sectional radius of the two lobes (approximately 50 Å). To remove this feature, models were constructed that were more "filled in", i.e., models which had less space in between the subunits. In order to retain some sense of the bilobal shape seen in the images, and at the same time remove the distinct separations between the lobes that give rise to the troublesome peak in the $P(r)$ function, a model with 4-fold symmetry was constructed from a central disk with four semiellipsoids at the periphery of the disk. Initially, the dimensions of the central disk and the semiellipsoids were chosen such that the outline of the model best fit one of the planar electron microscope images. The thickness of the model was chosen to give a reasonable value for the volume of the molecule. Again this type of model could yield the correct R_g and d_{max} values, but there was a strong peak in the model $P(r)$ at a value close to half the thickness of the disk. One way of removing this feature is to allow the thickness of the model to vary. In the absence of any data on the profile of PhK in this third dimension, the central disk was simply replaced with an oblate ellipsoid. This model was refined against the scattering data by manually adjusting the parameters: the dimensions of the central ellipsoid, the dimensions of the semiellipsoids, and the positions of the ellipsoids on the periphery of the central ellipsoid. The geometrical parameters for the resulting "best" model are given in Table II, and a sketch of its planar projection is shown in Figure 4. Figure 2 shows the good agreement between the experimental neutron-scattering intensity data and its $P(r)$ function and those predicted by the model.

The model shown in Figure 4 has planar dimensions that agree best with the TEM images of negatively stained samples published by Trempe et al. (1986). If the model structure is approximated by two lobes shaped as parentheses, the dimensions of the parentheses are approximately 250 × 105 Å

Table II: Geometrical Parameters for the "Best Fit" PhK Model[a]

major ellipse			
semiaxes	a = 105 Å	b = 105 Å	c = 40 Å
center	x = 0 Å	y = 0 Å	z = 0 Å
four semiellipsoids			
semiaxes	a = 60 Å	b = 54 Å	c = 42.5 Å
centers	x = 60 Å	y = 80 Å	z = 0 Å
	x = 60 Å	y = −80 Å	z = 0 Å
	x = −60 Å	y = −80 Å	z = 0 Å
	x = −60 Å	y = 80 Å	z = 0 Å
rotations about	x = 90°	y = 0°	z = 35°
	x = 90°	y = 0°	z = 145°
	x = 90°	y = 0°	z = 215°
	x = 90°	y = 0°	z = 325°

[a] In each case the ellipsoid or semiellipsoids are initially placed with their c axis aligned along z and their centers at (0,0,0). Their centers are then rotated and translated as indicated by the coordinates given above. The semiellipse centers are defined in the plane of their bases.

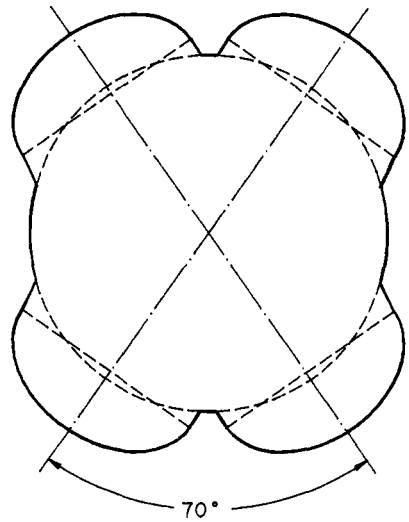

FIGURE 4: Planar projection of the model of PhK that best fits the neutron-scattering data. The dotted lines show the outlines of the ellipsoids and semiellipsoids used to construct the model.

with a maximum planar dimension of 285 Å. It is important to note that the two-dimensional planar images of PhK from TEM and STEM give no information about the thickness or variation of thickness in the third dimension. The model structure has the correct radius of gyration thickness, R_t, value in addition to the correct R_g, $P(r)$, and d_{max} values, indicating that the model represents a good approximation to the average variation in thickness. The fine details of the profile in the third dimension, however, remain subject to uncertainty without corroborative data from another technique. The smaller planar dimensions of the STEM images of unstained PhK consistently led to models that gave R_g values that were significantly smaller than the experimental values. One feature of the electron microscope images that is not included in the model is a narrow central hole arising from the fact that the two lobes of the structure appear to be bridged by two features that have dimensions of approximately 20 × 60 Å. These features are too small to be discernible by small-angle scattering, and attempts to include them did not affect the model fit in the accessible Q range.

Solution scattering data is spherically averaged due to the random orientations of the molecules. Thus it is not generally possible to prove a single model structure correct using scattering data alone. However, the various published images of PhK provide a guide for constructing models, and the scattering data provide an important test of any model based on these images. The most recent AFM and STM published images of PhK (Edstrom et al., 1990) have planar dimensions that are significantly larger than the scattering data allow. The AFM and STM images were produced from samples prepared by drying solutions of protein onto a graphite surface. The current state of development of both AFM and STM is such that we still do not understand all the possible sources of artifacts for these techniques, particularly when applied to biological macromolecules. The scattering data provide important structural constraints on PhK that may provide insights into the interpretation of the AFM and STM images. It is interesting that the model that has been found to agree best with the scattering data is in good qualitative agreement with the TEM images of negatively stained PhK (Trempe et al., 1986). This model provides a good starting point for further neutron-scattering studies of phosphorylase kinase reconstituted with deuterated subunits in order to locate specific subunits within the molecular boundary.

Acknowledgments

Thanks to Larry Garetto for preparing the original PhK samples for the neutron scattering experiments and to J. D. Smith for the drawings of the PhK model.

Registry No. Phosphorylase kinase, 9001-88-1.

References

Babu, Y. S., Bugg, C. E., & Cook, W. J. (1988) *J. Mol. Biol. 204*, 191.

Cohen, P. (1978) *Curr. Top. Cell. Regul. 14*, 117.

Edstrom, R. D., Meinke, M. H., Yang, X., Yang, R., & Fennell-Evans, D., (1989) *Biochemistry 28*, 4939.

Edstrom, R. D., Meinke, M. H., Yang, X., Yang, R., Eilings, V., & Fennel Evans, D. (1990) *Biophys. J. 58*, 1437.

Glatter, O. (1982) in *Small Angle X-ray Scattering*, (Glatter, O., & Kratky, O., Eds.) Chapter 4, pp 119–166, Academic Press, New York.

Guinier, A. (1939) *Ann. Phys. (Paris) 12*, 161.

Heidorn, D. B., & Trewhella, J. (1988) *Biochemistry 27*, 909.

Heidorn, D. B., & Trewhella, J. (1990) *Comments Mol. Cell. Biophys. 6*, 329.

Heidorn, D. B., Seeger, P. A., Rokop, S. E., Blumenthal, D. K., Means, A. R., Crespi, H., & Trewhella, J. (1989) *Biochemistry 28*, 6757.

Jennissen, H. P., & Schramm, H. J. (1981) *Biochem. Soc. Trans. 9*, 141.

Kringbaum, W. R., & Kugler, F. R. (1970) *Biochemistry 9*, 1216.

La Porte, D. C., Wierman, B. C., & Storm, D. R. (1980) *Biochemistry 24*, 8152.

Moore, P. B. (1980) *J. Appl. Crystallogr. 13*, 168.

Pickett-Gies, C. A., & Walsh, D. A. (1985) *J. Biol. Chem. 260*, 2046.

Pickett-Gies, C. A., & Walsh, D. A. (1986) *Enzymes (3rd ed.) 17*, 396.

Ramachandran, C., Goris, J., Waelkens, E., Merlevede, W., & Walsh, D. A. (1987) *J. Biol. Chem. 262*, 3210.

Schramm, H. J., & Jennissen, H. P. (1985) *J. Mol. Biol. 181*, 503.

Seeger, P. A., Hjelm, R. P., & Nutter, M. J. (1990) *Mol. Cryst. Liq. Cryst. 180A*, 101.

Tanaka, T., & Hidaka, H. (1980) *J. Biol. Chem. 255*, 11078.

Trempe, M. R., Carlson, G. M., Hainfeld, J. F., Furcinitti, P. S., & Wall, J. S. (1986) *J. Biol. Chem. 261*, 2882.

Trewhella, J., Blumenthal, D. K., Rokop, S. E., & Seeger, P. A. (1990) *Biochemistry 29*, 9316.

Zaccai, G., Wachtel, E., & Eisenberg, H. (1986) *J. Mol. Biol. 190*, 97.